NASA TECHNICAL NOTE

NASA TN D-7659

NASA TN D-7659

BASIC PERFORMANCE OF A MULTILAYER INSULATION SYSTEM CONTAINING 20 TO 160 LAYERS

by Robert J. Stochl

Lewis Research Center
Cleveland, Ohio 44135

NATIONAL AERONAUTICS AND SPACE ADMINISTRATION • WASHINGTON, D. C. • APRIL 1974

1. Report No.	2. Government Accession No.	3. Recipient's Catalog No.
NASA TN D-7659		

4. Title and Subtitle	5. Report Date
BASIC PERFORMANCE OF A MULTILAYER INSULATION SYSTEM CONTAINING 20 TO 160 LAYERS	APRIL 1974
	6. Performing Organization Code
7. Author(s)	8. Performing Organization Report No.
Robert J. Stochl	E-7815
	10. Work Unit No.
9. Performing Organization Name and Address	180-31
Lewis Research Center National Aeronautics and Space Administration Cleveland, Ohio 44135	11. Contract or Grant No.
	13. Type of Report and Period Covered
12. Sponsoring Agency Name and Address	Technical Note
National Aeronautics and Space Administration Washington, D.C. 20546	14. Sponsoring Agency Code

15. Supplementary Notes

16. Abstract

An experimental investigation was conducted to determine the thermal effectiveness of an aluminized Mylar-silk net insulation system containing up to 160 layers. The experimentally measured heat flux was compared with results predicted by using (1) a previously developed semi-empirical equation and (2) an effective-thermal-conductivity value. All tests were conducted at a nominal hot-boundary temperature of 294 K (530° R) with liquid hydrogen as the heat sink. The experimental results show that the insulation performed as expected and that both the semi-empirical equation and effective thermal conductivity of a small number of layers were adequate in predicting the thermal performance of a large number of layers of insulation.

17. Key Words (Suggested by Author(s))

Multilayer insulation
Insulation
Propellant storage

18. Distribution Statement

Unclassified - unlimited
Category 28

19. Security Classif. (of this report)	20. Security Classif. (of this page)	21. No. of Pages	22. Price*
Unclassified	Unclassified	26	$3.25

* For sale by the National Technical Information Service, Springfield, Virginia 22151

BASIC PERFORMANCE OF A MULTILAYER INSULATION SYSTEM CONTAINING 20 TO 160 LAYERS

by Robert J. Stochl

Lewis Research Center

SUMMARY

An experimental investigation was conducted to determine the thermal effectiveness of an aluminized Mylar-silk net multilayer insulation system containing up to 160 layers. The experimentally measured heat flux was compared with that predicted by using (1) a previously developed semiempirical equation which is applicable to any number of layers and (2) an effective-thermal-conductivity value based on the minimum number of layers tested and subsequently used to predict the performance of larger numbers of layers. The insulation system consisted of 20, 40, 60, 100, or 160 layers of aluminized Mylar with silk net spacers spirally wrapped around a cylindrical calorimeter. All tests were conducted at a nominal hot-boundary temperature of 294 K (530° R) with liquid hydrogen as the heat sink.

The experimental results indicate an exponentially decreasing normal heat flux for increasing numbers of layers, with approximately 71 percent of the decrease achieved with 60 layers.

Both methods used to predict the thermal performance of multilayer insulation systems of 20 to 100 layers predicted heat flux less than the actual heat flux by 0.2 to 7.1 percent. However, both methods predicted heat flux greater than the actual heat flux for the 160-layer test by 24.1 and 32.5 percent.

INTRODUCTION

The advent of high-energy upper-stage vehicles and long-duration, planetary orbit missions has led to the development of multilayer insulation (MLI) for use in cryogenic storage. Investigators have shown (e.g., refs. 1 and 2) that MLI is very effective in reducing radiant heat transfer to a cryogenic propellant tank, which for long-duration missions can be the major mode of heat transfer.

Two of the more important parameters that affect the thermal performance of MLI

systems are the total number of layers of insulation and the layer density. Advanced studies have indicated that from 100 to 200 layers of insulation may be required to achieve the thermal performance necessary for cryogenic storage during long-duration missions. Most thermal performance predictions to date are based on either effective thermal conductivity values or semiempirical equations. However, the first of these methods has been experimentally verified for only 30 layers or less of insulation. (The second method has been verified up to 112 layers.) It was questionable whether these conductivity values or equations would be applicable for 150- to 200-layer systems because of the possible effects of self-compression, trapped gases, and installation techniques.

The purpose of this report is to present the results of an investigation conducted at the NASA Lewis Research Center to (1) obtain experimental heat-transfer data on a particular insulation system containing a large number of layers, (2) determine whether the semiempirical equations developed in reference 1 can be used to predict the heat transfer through larger number of layers, and (3) determine whether an effective-thermal-conductivity value based on a few layers can be used to predict the performance of larger numbers of layers. Double-aluminized Mylar with silk net spacers was used in various thicknesses from 20 to 160 layers at an average density of 20.5 layers per centimeter (52 layers/in.). The insulation was spirally wrapped onto a 0.762-meter-(30-in.-) diameter cylindrical calorimeter. The purpose of the spiral wrapping was to eliminate the discontinuities associated with insulation blankets. Five tests were conducted on the insulation system with (sequentially) 160, 100, 60, 40, and 20 layers of insulation. The tests were conducted at a nominal hot-boundary temperature of 294 K (530° R) with liquid hydrogen as the low-temperature heat sink.

The tests were conducted under a vacuum of 10^{-6} torr to minimize any heat transfer due to gas conduction within the insulation. The parameter used to evaluate the thermal performance of the insulation system was the normal heat flux through the MLI.

SYMBOLS

A	empirical constant
$A_{\log\ mean}$	log mean area, $(A_2-A_1)/\ln (A_2-A_1)$, m^2; ft^2
A_m	cross-sectional area of metallic film, m^2; ft^2
A_T	surface area of measure tank, m^2; ft^2
A_1	area of innermost layer of insulation, m^2; ft^2
A_2	area of outer layer of insulation, m^2; ft^2
B	empirical constant

C	empirical constant
C_v	specific heat at constant volume, J/(kg)(K); Btu/(lb)(^oR)
g	gravity acceleration, m/sec^2; ft/sec^2
h	specific enthalpy, J/kg; Btu/lb
k_{eff}	effective thermal conductivity, W/(m)(K); Btu/(hr)(ft)(^oR)
k_m	thermal conductivity of thin aluminum film, W/(m)(K); (Btu/(hr)(ft)(^oR)
Δl	increment of length, m; ft
m	mass, kg; lb
$\dot{m}$	mass flow rate, kg/sec; lb/sec
N_S	total number of layers of insulation
$\overline{N}$	layer density, layers/cm; layers/in.
P	pressure, torr or N/cm^2; psia
Q	heat transfer, J; Btu
$\dot{Q}$	heat-transfer rate, W; Btu/hr
q	heat-transfer rate per unit area, W/m^2; Btu/(hr)(ft^2)
ΔR	differential length in radial (normal) direction, m; ft
r	empirical constant (exponent)
S	empirical constant (exponent)
ΔS	differential length in circumferential direction, m; ft
T	temperature, K; ^oR
T_m	mean temperature, K; ^oR
t	time, sec
U	internal energy, J; Btu
u	specific internal energy, J/kg; Btu/lb
V	velocity, m/sec; ft/sec
v	specific volume, m^3/kg; ft^3/lb
W	work, J; Btu
Z	elevation, m; ft
λ	latent heat of vaporization, J/kg; Btu/lb

σ	Stefan-Boltzmann constant, 5.668×10^{-8} W/(m^2)(K^4); 1.714×10^{-9} Btu/(hr)(ft^2)(R^4)

Subscripts:

c	cold boundary
f	final time
G	ullage gas
H	hot boundary
i	initial time
L	lateral direction
l	liquid
M	miscellaneous
N	normal direction
o	leaving system
S	circumferential direction
SH	superheating
SL	saturated liquid
SV	saturated vapor
SYSTEM	total system
T	total quantity
W	wall

EXPERIMENTAL APPARATUS

Facility

All tests were conducted inside a 7.61-meter- (25-ft-) diameter spherical vacuum chamber (fig. 1) in order to minimize heat transfer by gaseous conduction and convection. The vacuum capability of this chamber was approximately 8×10^{-7} torr.

A general schematic of the cylindrical calorimeter and associated equipment is shown in figure 2. The calorimeter was placed vertically inside a cylindrical shroud 2.44 meters (8 ft) in diameter and 2.44 meters (8 ft) in length. Electric strip heaters were attached to the exterior of the shroud to provide the constant warm-boundary temperature.

The pressures inside the measure tank and cold-guard tanks were controlled by separate closed-loop systems capable of maintaining each pressure within 1.4×10^{-4} newton per square centimeter (0.0002 psia) of a desired value. These pressure-control systems, shown schematically in figure 2, consisted of high-resolution differential-pressure transducers which sensed very small pressure variations inside the tanks relative to an absolute reference pressure. The electrical output signals from the transducers were transmitted to control units for electrohydraulic pressure regulating valves in the respective vent lines. The reference pressure was provided by a fixed volume of gaseous nitrogen maintained at a constant temperature by an ice bath. The pressure inside the measure and guard tanks was maintained at 12.05 and 12.06 newtons per square centimeter (17.48 and 17.50 psia), respectively. The higher pressure in the cold-guard tanks (with its higher saturation temperature) prevented condensation of the vaporized measure tank gas as it passed through the upper cold-guard tank.

The total heat transfer to the measure tank was determined by one of five mass flowmeters measuring the boiloff rate. The steady-state heat-transfer rate was directly proportional to the gas flow rate since the measure tank pressure was held within $\pm1.4\times10^{-4}$ newton per square centimeter (0.0002 psia). The meter for the smallest flow rate had a capacity of 0.00283 standard cubic meter per hour (0.1 standard ft^3/hr), and each succeeding meter differed in capacity by a factor of 10.

Calorimeter

The calorimeter, shown in figure 3, consisted of three separate 76.2-centimeter-(30.0-in.-) diameter tanks. The measure tank was 76.2 centimeters (30.0 in.) in length and was located between two cold guards. The cold guards served to eliminate heat flow into the measure tank through its two ends and to minimize insulation edge effects on heat-transfer measurements. The calorimeter was constructed of 1.27-centimeter-(0.5-in.-) thick 1100-alloy aluminum.

The measure and cold-guard tanks were supported through their centers by a stainless-steel tube. During a test this support tube was filled with liquid hydrogen to prevent any conduction or radiation from reaching the measure tank. Laminated thermoplastic spacers were used to (1) separate the tanks from each other and from the support tube and (2) center the fill and vent tubes that passed through the tanks. Copper wool was packed into the annular space around all tubes that penetrated the upper guard tank to provide a good thermal heat path and thus further reduce possible conduction into the measure tank along these tubes.

A plastic ring was attached to each cold guard near the end to provide a means of support for the insulation. A polyurethane foam cap, approximately 3.8 centimeters (1.5 in.) thick and with a density of 32 kilograms per cubic meter (2 lb/ft^3), was formed

around the end of each cold guard to reduce the heat flux into the guard tanks. These foam caps were covered with aluminized Mylar to reduce further the heat flux being radiated from the surroundings to the ends of the cold guards.

To assure a smooth surface for wrapping the insluation around the calorimeter, bands of thin, soft aluminum were placed around the gaps between the measure tank and the cold guards. A sheet of aluminized Mylar was bonded to the calorimeter (between the plastic rings) to provide a surface of known emissivity.

Insulation System

The insulation system consisted of a continuous sheet of double-aluminized Mylar spirally wrapped around the calorimeter between the two plastic rings. Each layer of Mylar was separated from the next by two layers of silk net. The double-aluminized Mylar was 1.52 meters (60 in.) wide and 0.00063 centimeter (1/4 mil) thick. The Mylar had between 300×10^{-10} and 500×10^{-10} meter (300 and 500 Å) of aluminum on each side and measured room-temperature emittance values between 0.022 and 0.030. The silk netting was also 1.52 meters (60 in.) wide, had a 14 by 14 mesh, and was approximately 0.010 centimeter (0.004 in.) thick.

The method and equipment used to wrap the insulation around the calorimeter are shown in figure 4. A constant tension was maintained on the aluminized Mylar while the calorimeter was rotated to ensure that the alternate sheets of aluminized Mylar and silk netting were wrapped at nearly constant layer density. A total of 160 layers of insulation were applied to the tank at an average layer density of 20.5 layers per centimeter (52 layers/in.). A braided Dacron string was taped to every tenth layer of the aluminized Mylar and attached to the plastic ring at each end of the calorimeter, as shown in figure 5, to help support the insulation when in the vertical position and also to help prevent the layers from unwinding. Also shown in figure 5 is one of four flattened stainless-steel tubes. Each tube was 0.80 meter (31.5 in.) long, had an outside diameter of 0.953 centimeter (0.375 in.) flattened to 0.203 centimeter (0.080 in.), and had a wall thickness of 0.036 centimeter (0.014 in.).

One tube was installed next to the tank and one tube at each of the 20-, 60-, and 100-layer positions. The purpose of these tubes was to allow the determination of the interstitial pressure within the insulation. The open end of each tube was located halfway down the measure tank. The pressure at the other end of the tube was sensed by ionization gages.

Instrumentation

Instrumentation was provided for measuring insulation and shroud temperatures, temperatures at various locations on the test hardware, pressures of the measure and cold-guard tanks, pressure in the vacuum chamber, and vaporization rate from the measure tank.

The insulation temperatures were obtained with copper-constantan thermocouples. Sixty-three 32 gage (0.020-cm- (0.008-in.-) diam) thermocouples were located throughout the insulation, as shown in figure 6, to give radial temperature profiles at two locations over the measure tank and one radial profile over each cold-guard tank. These thermocouple locations also gave lateral temperature profiles along the layers of the insulation.

The insulation temperatures had an uncertainty of ±5.6 K (10° R) at liquid-hydrogen temperature. This uncertainty improved to ±0.6 K (1° R) at room temperature.

Platinum resistance sensors were used to determine measure tank and cold-guard wall temperatures as well as temperatures inside these vessels. Platinum resistance sensors were also used for fill and vent line and shroud temperatures. These sensors had an uncertainty of ±0.06 K (0.1° R) at liquid-hydrogen temperatures.

Measure tank, cold-guard, and line pressures were measured with bonded strain-gage transducers which had an estimated uncertainty of ±1/4 percent.

The vacuum levels, both inside the shroud and in the spaces between the shroud and chamber and within the insulation, were determined by ionization gages.

The vaporization rate from the measure tank was metered by one of a series of five mass flowmeters. These meters were calibrated with gaseous hydrogen and had full-scale ranges of 0 to 0.0028, 0 to 0.028, 0 to 0.28, 0 to 2.83, and 0 to 28.3 standard cubic meter per hour (0.1, 1.0, 10.0, 100.0, and 1000 standard ft^3/hr). The uncertainty associated with these meters was ±1/2 percent.

All measurements were recorded on a high-speed digital data system.

PROCEDURE

In a typical experimental run the chamber was evacuated to approximately 1×10^{-6} torr and held at that level for at least 24 hours in order to evacuate the intersitital gases from the multilayer insulation. The chamber vacuum was then broken (to approximately 100 torr) with gaseous helium, and the chamber was reevacuated. This procedure was repeated twice to ensure a helium background in the chamber and insulation. The measure tank and cold guards were then filled with liquid hydrogen under a back pressure of approximately 20.69 newtons per square centimeter (30 psia). After all tank and vent line temperatures stabilized, the measure tank and cold guards were vented to their

normal operating pressures. This procedure served to ensure that the tanks contained saturated liquid. The measure and guard tank pressures were then controlled by the closed-loop perssure-control system to $12.05 \pm 1.4 \times 10^{-4}$ and $12.06 \pm 1.4 \times 10^{-4}$ newton per square centimeter (17.48 ± 0.0002 and 17.50 ± 0.0002 psia), respectively. The shroud temperature was then established and maintained at 294.0 ± 1.1 K ($530 \pm 2.0^{\circ}$ R) by a closed-loop temperature-control system.

Insulation temperatures and boiloff were monitored until steady-state thermal conditions were reached. It took approximately 5 days to reach steady state for the 160-layer system and approximately 3 days for the 20-layer system. Steady state was defined to occur when temperatures and boiloff did not vary by more than the error band of the measuring system based on a minimum of three consecutive readings spaced approximately 2 hours apart.

The test series began with 160 layers of insulation. Subsequent data points were obtained by unwrapping a given number of layers to form the next configuration (100, 60, 40, or 20 layers). The layers of insulation were removed by hand with extreme care to avoid disturbing the remaining insulation.

A null (or tare) test was performed in an attempt to determine the magnitude of possibly stray heat leaks into the measure tank. This test was conducted with liquid hydrogen in the measure and guard tanks and also in the shroud surrounding the calorimeter. This test was terminated when a steady boiloff was obtained and all temperatures were between those of the measure tank and the shroud.

DATA ANALYSIS

Experiment

Steady-state heat transfer through MLI systems consists of a combination of radiation and conduction. In addition to heat transfer normal to the insulation, heat can be transferred by (1) solid conduction laterally along the layers of insulation (edge effects) and (2) solid conduction circumferentially along the layers because of the spiral wrap technique. In this experimental test program heat also entered the measure tank by conduction across the aluminum bands, the spacer blocks between fill and vent lines, and the spacers between the guard tanks and measure tanks.

The parameter used as a measure of the effectiveness of the MLI system in subsequent discussions is the normal heat transfer (radiation and conduction) through the insulation. The normal heat transfer was obtained from the relation

$$\dot{Q}_N = \dot{Q}_T - \dot{Q}_M - \dot{Q}_L - \dot{Q}_S \tag{1}$$

The terms on the right side of equation (1) were evaluated as described in the paragraphs that follow.

Total heat transfer into measure tank. - For the thermodynamic system consisting of the entire tank and its contents (tank and ullage gas and liquid), the first law of thermodynamics for an increment of time dt may be written as

$$\delta Q_T - \delta m_o \left(u_o + P_o v_o + \frac{V_o^2}{2g} + Z_o \right) = dU_{SYSTEM} + \delta W \tag{2}$$

The kinetic and potential energy terms are small in comparison with the other energy terms and will be neglected in this development. For this system, there is no external work done on the system so $\delta W = 0$. If $h = u + pv$ is substituted, equation (2) becomes

$$\delta Q_T - \delta m_o h_o = dU_{SYSTEM} \tag{3}$$

Equation (3) can be integrated over any time period. The physical interpretation of the quantities in equation (3) is as follows:

$$\int_{t_i}^{t_f} \dot{Q}_T \, dt = \int_{t_i}^{t_f} \dot{m}_o h_o \, dt + \int_{U_{t_i}}^{U_{t_f}} dU_{SYSTEM} \tag{4}$$

Energy input through insulation	Energy leaving through vent gas	Change in system energy

Change in system energy. - The change in system energy can be separated into three categories, (1) change in ullage energy, (2) change in liquid energy, and (3) change in wall energy:

$$dU_{SYSTEM} = dU_G + dU_l + dU_W \tag{5}$$

Change in ullage energy. - The change in ullage or gas energy may be obtained by integration of the relation

$$\int_{U_{t_i}}^{U_{t_f}} dU_G = \int_{T_i}^{T_f} m_G C_{v_G} dT$$

over the ullage temperature profile at times t_i and t_f

Change in liquid energy. - The change in liquid energy, assuming that the liquid is completely saturated at the corresponding measure tank pressure (in this condition there would be no energy stored), can be evaluated by

$$dU_l = -\Delta m_l h_{SL}$$

where Δm_l is the amount of liquid evaporated.

Change in wall energy. - The change in wall energy may be obtained in a manner similar to the change in ullage energy:

$$\int_{U_{t_i}}^{U_{t_f}} dU_W = \int_{T_i}^{T_f} m_W C_{v_W} dT$$

From the temperature sensors used in this experimental program it was determined that neither the wall energy nor the ullage energy changed over the time period used to evaluate steady-state boiloffs. Therefore, only the liquid energy change was considered. Equation (4) then becomes

$$\int_{t_i}^{t_f} \dot{Q}_T dt = \int_{t_i}^{t_f} \dot{m}_o h_o dt - \int_{t_i}^{t_f} \dot{m}_l h_{SL} dt \tag{6}$$

or

$$\int_{t_i}^{t_f} \dot{Q}_T \, dt = \int_{t_i}^{t_f} (\dot{m}_o h_o - \dot{m}_l h_{SL}) dt \tag{7}$$

The enthalpy of the gas leaving the system h_o can be set equal to the enthalpy of saturated gas h_{SV} plus a certain amount of superheating h_{SH} which is a function of the temperature and pressure of the gas leaving the system. That is,

$$h_o = h_{SV} + h_{SH}$$

Also, the mass leaving the system m_o is equal to the change in liquid mass Δm_l minus the change in ullage mass Δm_G:

$$\dot{m}_o = \Delta \dot{m}_l - \Delta \dot{m}_G$$

For this report the rate of change in ullage mass during steady-state operation was small and could be considered zero, so that

$$\dot{m}_o = \Delta \dot{m}_l = \dot{m}_l$$

Substituting these values of $\dot{m}_o$ and h_o into equation (7) results in

$$\int_{t_i}^{t_f} \dot{Q}_T \, dt = \int_{t_i}^{t_f} \left[\dot{m}_l (h_{SV} + h_{SH}) - \dot{m}_l h_{SL} \right] dt$$

or

$$\int_{t_i}^{t_f} \dot{Q}_T \, dt = \int_{t_i}^{t_f} \dot{m}_l (\lambda + h_{SH}) dt \tag{8}$$

where latent heat of evaporation λ is equal to $h_{SV} - h_{SL}$. Equation (8) was used to determine the total heat input into the measure tank. The mass flow rate $\dot{m}_l$ was determined from the flowmeters. The latent heat of evaporation λ is a function of measure tank pressure, and the amount of superheat h_{SH} is a function of outlet temperature.

Lateral heat transfer. - The lateral heat flux $\dot{Q}_L$ was evaluated as follows:

$$\dot{Q}_L = \sum_{i=1}^{N_S} \left(A_m k_m \frac{\Delta T}{\Delta l} \right)_i \tag{9}$$

In this calculation the cross-sectional area of the insulation in the lateral direction was partitioned into a series of annular rings. Each annular ring contained 10 layers of insulation. The heat transfer through each ring was calculated and summed to give the total lateral heat transfer. The thermal conductivity values used in this calculation are for thin aluminum film, as reported in reference 3. The values given in reference 3 were curve fit to give the following relation:

$$k_m = 1.0263 + 0.0024\ T_m \tag{10}$$

Spiral heat transfer. - The solid-conduction circumferential heat transfer along the layers was determined by using the equation

$$\dot{Q}_S = A_m k_m \frac{\Delta T}{\Delta S} \tag{11}$$

For each test condition this equation was evaluated at the measure tank wall, where ΔT is the difference between the tank wall temperature and the temperature of the first shield 180° from the interface of the shield and the tank wall.

Miscellaneous heat transfer. - The heat transfer into the measure tank as a result of conduction across aluminum bands, spacers, and any unaccountable heat paths was lumped into a single value and considered to be constant for all experimental tests. This value, determined from the null test to be 0.032 watt (0.108 Btu/hr) was subtracted from the measured heat transfer $\dot{Q}_T$ of each test to give the term $\dot{Q}_T - \dot{Q}_m$ in equation (1).

Predicted Results

The experimental results obtained from equations (1) to (11) are compared in this report with results predicted by using two separate methods.

Method 1. - Method 1 uses the semiempirical relation developed in reference 1. In reference 1 an analytical expression was derived which described the one-dimensional thermal performance of multilayer insulations. The generalized relation for the total heat flux normal to the insulation layers was given as

$$q = \frac{CP(X,T)\left(T_H^{r+1} - T_c^{r+1}\right)}{(N_s + 1)(r + 1)} + \frac{A\bar{N}^s T_m (T_H - T_c)}{N_s + 1} + \frac{B\sigma\left(T_H^{4.67} - T_c^{4.67}\right)}{N_s} \qquad (12)$$

Gas conduction component | Solid conduction component | Radiation component

where $P(X, T)$ is the pressure within the insulation as a function of position and local temperature, and the coefficients A, B, and C and the exponents r and s are evaluated from experimental information on a particular insulation system and interstitial gas. The values used for comparisons in this report are those obtained in reference 1 for an insulation system consisting of unperforated, 6.35×10^{-4}-centimeter (1/4-mil) double-aluminized Mylar with double silk net spacers and helium as the interstitial gas. For this system equation (12) becomes

$$q = \frac{4.886\times10^{4}\, P\left(T_H^{0.26} - T_c^{0.26}\right)}{N_s} + \frac{8.953\times10^{-8}\, N^{2.56}\, T_m (T_H - T_c)}{N_s} + \frac{2.953\times10^{-4}\,\sigma\left(T_H^{4.67} - T_c^{4.67}\right)}{N_s} \qquad (13)$$

where P is the pressure in torr. The denominator of both conduction terms becomes N_s rather than $N_s + 1$ because of the use of the exterior shield temperature as the warm-boundary temperature.

Method 2. - Method 2 is based on using an effective thermal conductivity value, which satisfies the general solid conduction equation for a given set of experimental results, to predict the results of the other experimental data.

The particular effective thermal conductivity value used in this report was obtained from the experimental results of the 20-layer test and is defined as

$$k_{eff} = \left(\frac{\dot{Q}_N \Delta R}{A_{\log\ mean}\, \Delta T}\right)_{N_s=20} \qquad (14)$$

where $\Delta R = N_S/N$, so that

$$k_{eff} = \left[\frac{\dot{Q}_N \left(\ln \frac{A_2}{A_1} \right) N_S}{\Delta T (A_2 - A_1) \overline{N}} \right]_{N_S=20} \tag{15}$$

The heat flux values for the other thicknesses were then obtained by using the equation

$$q = \frac{A_{\log \text{ mean}}}{A_T} k_{eff} \frac{\overline{N}}{N_S} (T_H - T_C) \tag{16}$$

RESULTS AND DISCUSSION

Steady-state test data for the five insulation thicknesses are given in table I. The measured heat flux (corrected for the null test) into the measure tank is shown in column 5 of table I and plotted in figure 7 as a function of the number of layers of insulation. The corrected normal heat flux (column 8 of table I) is also shown to indicate the magnitude of the corrections for lateral and spiral heat leak that were applied to the measured heat flux. Figure 7 indicates an exponentially decreasing heat flux for increasing numbers of layers of insulation, where approximately 78 and 71 percent of the measured and normal heat-flux reductions (going from 20 to 160 layers) are achieved with 60 layers of insulation.

As mentioned in the section Experiment, the parameter used as a measure of the effectiveness of the various MLI systems is the corrected normal heat flux through the insulation (column 8 of table I). Figure 8 presents a comparison of experimental and predicted normal heat-flux values as a function of the number of layers. The agreement between the experimental results and the results of both methods of prediction is good except for the 160 layers of insulation. The results predicted by the semiempirical relation (eq. (13)) are presented in its three component parts: a radiation component, a solid conduction component, and a gas conduction component. This relation indicates that an average of 28, 48, and 24 percent of the total normal heat flux is due to radiation, solid conduction, and gas conduction, respectively, for all systems. The rather large percent due to gas conduction is the result of using the average measured interstitial pressure of 4×10^{-5} torr. The tube and ionization gage assemblies that were located within the insulation system indicated at least an order of magnitude higher pressure

than was recorded outside the system. This could be the result of (1) the facility not providing the pressure differential required to evacuate the insulation (lowest obtainable chamber vacuum was 1×10^{-6} torr during testing), (2) the insulation technique not providing adequate molecular venting paths, or (3) a combination of the first two effects.

The deviations between the experimental and predicted results are listed in table II. The discrepancy between the experimental results and the results predicted by using equation (13) varies from an overprediction of 24.1 percent for 160 layers to an underprediction of 6.6 percent for 40 layers. These results are generally within the degree of predictability reported in reference 1. It should be noted here that the experimental normal heat-flux value for the 160-layer test was obtained after a rather large correction for lateral heat transfer, where 58 percent of the measured heat-transfer value was due to lateral conduction. Therefore, the uncertainty associated with presenting this experimental value and comparing it with the predicted result is much larger than it is for the other thicknesses.

The second method used to predict the normal heat flux is based on using an effective-thermal-conductivity value which is based on the experimental results obtained from the 20-layer system. As can be seen in figure 8 and table II, this method produces results which are similar to those obtained by using equation (13). The discrepancy between results for this method and the experimental results for 160 layers could again be due to the large uncertainty associated with this particular experimental result.

The temperatures which were measured through the insulation for each configuration are presented in figure 9 and table III. It can be seen from inspection of figure 8 that the profiles for the 60-, 100-, and 160-layer configurations are S-shaped, while the other two are slightly convex. Although this effect is not completely understood, one possible explanation is a nonuniform layer density through the original 160 layers of insulation inasmuch as the S-shaped profile is not present in the lesser numbers of layers.

Generally, both methods shown are capable of predicting heat flux to within 10 percent of that obtained experimentally. However, using an effective-thermal-conductivity value limits its use to systems which have the layer density, boundary temperatures, and interstitital pressure for which it was originally evaluated.

SUMMARY OF RESULTS

An experimental investigation was conducted to (1) obtain data on a particular insulation system containing a large number of layers of insulation, (2) determine whether the semiempirical equation developed in NASA CR-130678 is applicable to these large numbers of layers, and (3) determine whether an effective-thermal-conductivity value based on a few layers can be used to predict the performance of larger numbers of layers. The insulation system consisted of various numbers of layers (20 to 160) of

aluminized Mylar with silk net spacers spirally wrapped around a cylindrical calorimeter. All tests were conducted at a nominal hot-boundary temperature of 294 K (530° R) with liquid hydrogen as the heat sink. The following results were obtained:

1. The total heat flux decreased exponentially for increasing numbers of layers of insulation. Approximately 71 percent of the normal heat-flux reduction, achieved in going from 20 to 160 layers, was obatined with 60 layers of insulation.

2. Predicted heat-flux values obtained by using the semiempirical equation were between 0.6 and 6.6 percent less than those obtained experimentally for the 20- to 100-layer configurations and 24.1 percent greater than that for the 160-layer configuration.

3. Calculations of heat flux, based on the overall thermal-conductivity value obtained from the 20-layer configuration, were 0.2 to 7.1 percent less than those obtained experimentally for the 20- to 100-layer configurations and 32.5 percent greater than that for the 160-layer configuration.

4. The large deviations between the experimental and predicted results for the 160-layer test were due to the large amount of lateral conduction (edge effects) encountered in this particular test. However, in the absence of edge effects, it would be expected that the deviation between the experimental and predicted results for the 160-layer test would be comparable to those obtained for the other thicknesses.

5. In general, the insulation performed as expected.

6. Both the semiempirical equation and the effective thermal conductivity of a small number of layers (20) were adequate in predicting the thermal performance of a large number of layers ($\leq$160).

Lewis Research Center,
National Aeronautics and Space Administration,
Cleveland, Ohio, January 10, 1974,
180-31.

REFERENCES

1. Keller, C. W.: Thermal Performance of Multilayer Insulations. Sixth Quarterly Activity Report, LMSC-D337102, Lockheed Missiles and Space Co. (NASA CR-130678), 1972.

2. Folkman, N. R.; and Lee, T. G.: Thermodynamic Design Fundamentals of High-Performance Insulation. Jour. Spacecraft and Rockets, vol. 5, no. 8, Aug. 1968, pp. 954-959.

3. Tien, C. L.; Jagannathan, P. S.; and Chan, C. K.: Lateral Heat Transfer in Cryogenic Multilayer Insulation. Volume 18 of Advances in Cryogenic Engineering, K. D. Timmerhaus, ed., Plenum Press, 1973, pp. 118-123.

TABLE I. - SUMMARY OF EXPERIMENTAL RESULTS

1	2		3		4		5		6		7		8		9	
Number of layers	Warm boundary temperature		Cold boundary temperature		Average layer density		Measured heat flux		Lateral heat-transfer correction		Spiral heat-transfer correction		Corrected normal heat flux, column 5 - column 6 + column 7		Overall effective thermal conductivity	
	K	^{o}R	K	^{o}R	layers/cm	layers/in.	W/m^2	$Btu/(hr)(ft^2)$	W/m^2	$Btu/(hr)(ft^2)$	W/m^2	$Btu/(hr)(ft^2)$	W/m^2	$Btu/(hr)(ft^2)$	W/m^2	$Btu/(hr)(ft)(^{o}R)$
160	292.7	527	20.9	37.6	20.5	52.0	0.2198	0.0697	0.1268	0.0402	8.7×10^{-5}	2.8×10^{-5}	0.0929	0.0295	2.429×10^{-5}	1.404×10^{-5}
100	290.3	522.5	20.9	37.6	20.5	52.0	.2816	.0893	.0928	.0294	6.4×10^{-5}	2.0	.1888	.0599	3.228	1.866
60	293.6	528.1	20.9	37.6	20.5	52.0	.3621	.1148	.0433	.0138	1.4×10^{-4}	4.5	.3186	.1010	3.311	1.914
40	293	527.4	20.9	37.6	20.5	52.0	.5184	.1645	.0234	.0074	2.1×10^{-4}	6.5	.4949	.1570	3.465	2.003
20	285.4	513.7	20.9	37.6	20.2	51.3	.8814	.2796	.0088	.0028	2.6×10^{-4}	8.2	.8720	.2767	3.220	1.861

TABLE II. - DEVIATIONS BETWEEN EXPERIMENTAL AND PREDICTED HEAT-FLUX RESULTS

1	2		3		4	5		6
Number of layers	Experimental results		Results predicted by eq. (13)		Percent deviation between columns 2 and 3, $\frac{\text{column 2 - column 3}}{\text{column 2}} \times 100$	Predicted results based on using effective thermal conductivity of 20-layer test		Percent deviation between columns 2 and 5, $\frac{\text{column 2 - column 5}}{\text{column 2}} \times 100$
	W/m^2	$Btu/(hr)(ft^2)$	W/m^2	$Btu/(hr)(ft^2)$		W/m^2	$Btu/(hr)(ft^2)$	
160	0.0929	0.0295	0.1153	0.0366	-24.1	0.1233	0.0391	-32.5
100	.1888	.0599	.1807	.0573	4.3	.1885	.0598	.2
60	.3186	.1010	.3091	.0981	2.9	.3105	.0985	2.5
40	.4949	.1570	.4622	.1466	6.6	.4596	.1458	7.1
20	.8720	.2767	.8532	.2707	.6	.8720	.2767	----

TABLE III. - TEMPERATURES THROUGH MULTILAYER INSULATION

Layer	Layers in configuration									
	160		100		60		40		20	
	Layer temperature									
	K	°R	K	°R	K	°R	K	°R	K	°R
1	38.4	69.2	68.0	122.4	52.4	94.4	72.1	129.7	125.1	225.2
2	52.5	94.5	88.0	158.3	76.0	136.7	101.2	182.3	154.6	278.3
3	65.7	118.1	103.8	186.8	93.6	168.5	120.9	217.8	171.5	308.7
5	83.7	150.5	125.5	225.9	120.0	216.3	147.0	264.7	----	----
8	113.0	203.6	150.2	270.4	151.4	272.5	171.2	308.2	223.3	402.0
9	121.0	217.9	154.9	278.8	158.5	285.2	178.2	320.9	229.2	412.6
10	127.2	229.0	159.6	287.3	164.8	296.9	184.0	331.2	235.2	423.3
16	156.4	281.5	179.7	323.4	194.3	349.8	212.0	381.9	265.3	477.6
18	165.5	297.7	184.1	331.2	203.1	365.9	221.9	399.4	275.1	495.2
20	171.4	308.7	188.9	340.0	210.7	379.3	230	414.0	285.4	513.7
36	204.5	368.4	212.8	383.1	249.5	449.2	281.5	506.9	----	----
38	207.2	373.2	215.1	387.1	253.0	455.8	287.0	516.5	----	----
40	209.0	376.5	217.3	391.2	256.2	461.7	293.0	527.4	----	----
54	223.0	401.3	232.4	418.4	281.5	506.8	----	----	----	----
57	225.5	406.1	235.1	423.2	287.0	516.6	----	----	----	----
60	228.0	410.4	237.9	428.2	293.6	528.1	----	----	----	----
74	238.5	429.5	252.2	454.0	----	----	----	----	----	----
77	240.4	432.9	255.2	459.4	----	----	----	----	----	----
80	242.3	436.6	258.3	464.9	----	----	----	----	----	----
92	247.7	445.9	275.7	496.2	----	----	----	----	----	----
96	249.5	449.2	282.7	508.9	----	----	----	----	----	----
100	251.8	453.2	290.3	522.5	----	----	----	----	----	----
120	263.7	474.9	----	----	----	----	----	----	----	----
125	267.0	480.6	----	----	----	----	----	----	----	----
130	269.8	485.7	----	----	----	----	----	----	----	----
150	284.0	511.4	----	----	----	----	----	----	----	----
155	288.0	518.5	----	----	----	----	----	----	----	----
160	292.7	527.0	----	----	----	----	----	----	----	----

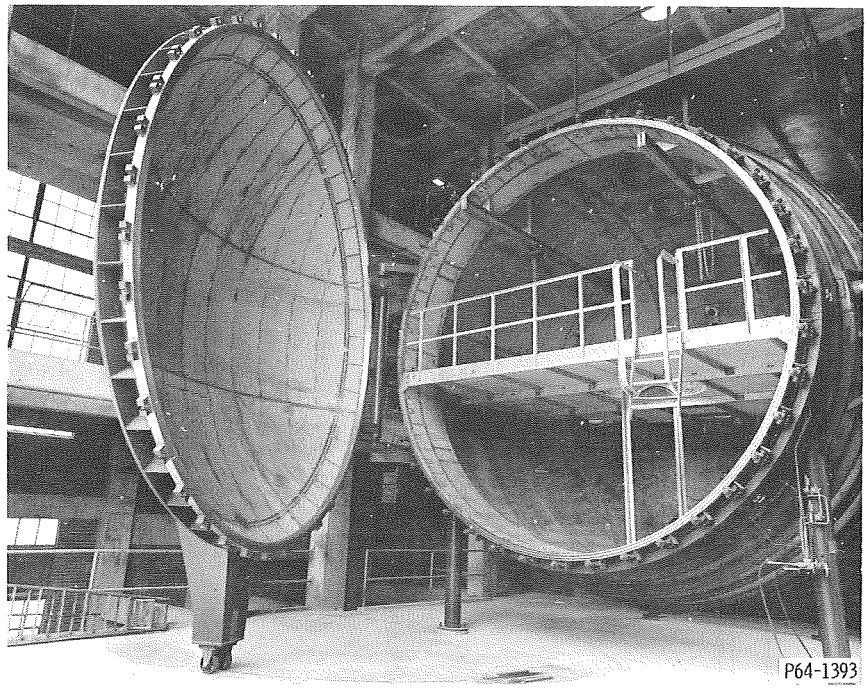

Figure 1. - Spherical 7.61-meter- (25-ft-) diameter vacuum chamber.

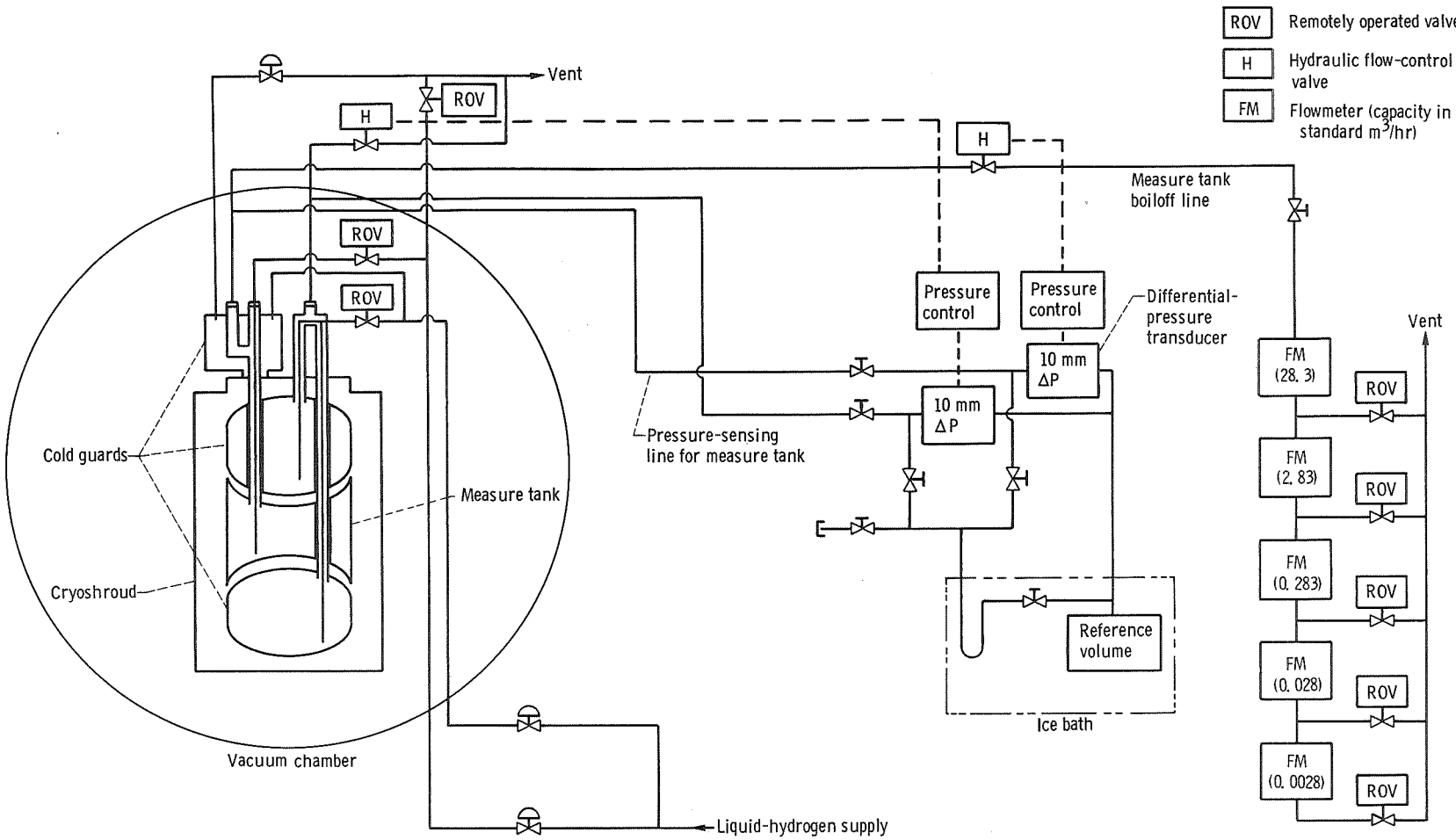

Figure 2. - General schematic of facility.

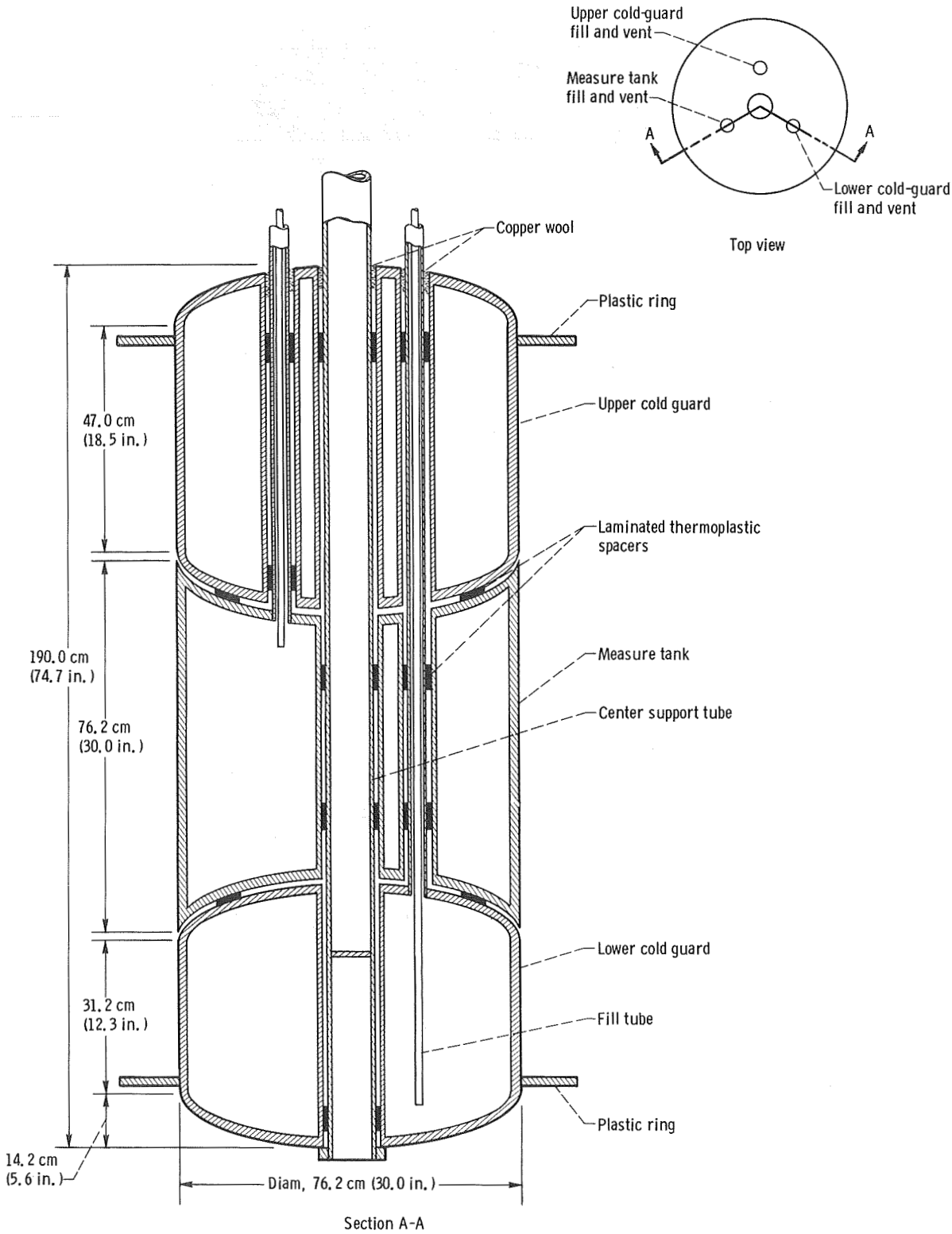

Figure 3. - Doubly guarded cylindrical calorimeter.

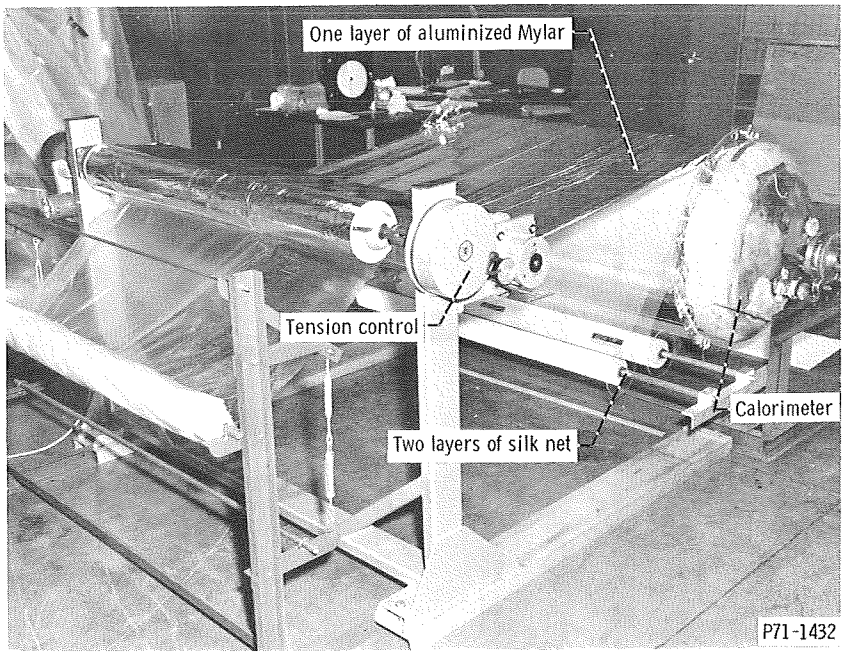

Figure 4. - Method used to spiral wrap insulation onto calorimeter.

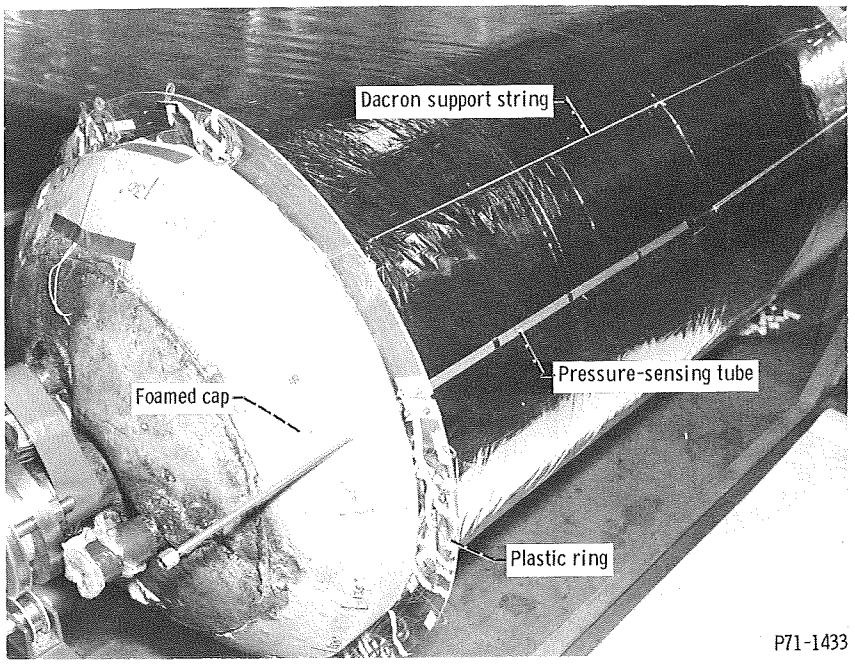

Figure 5. - Calorimeter insulation details.

Thermocouple locations

Location	Layer							
	1, 2, 3, 5, 8, 9, 10, 16, 18, 20	36, 38, 40	57	60, 74, 77, 80, 92	96	100, 120, 125, 130, 150	155	160
A	√		√		√		√	
B	√		√		√		√	
C	√	√	√	√	√	√	√	√
D	√							

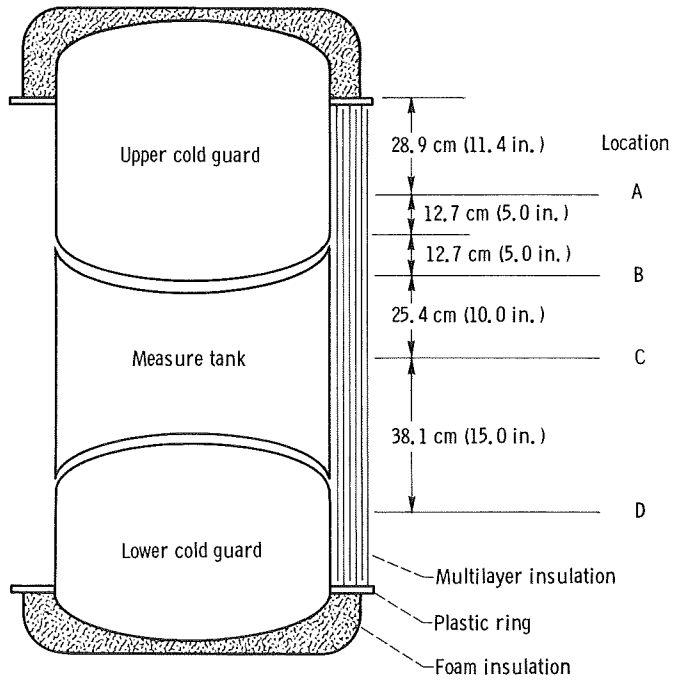

Figure 6. - Thermocouple locations within multilayer insulation.

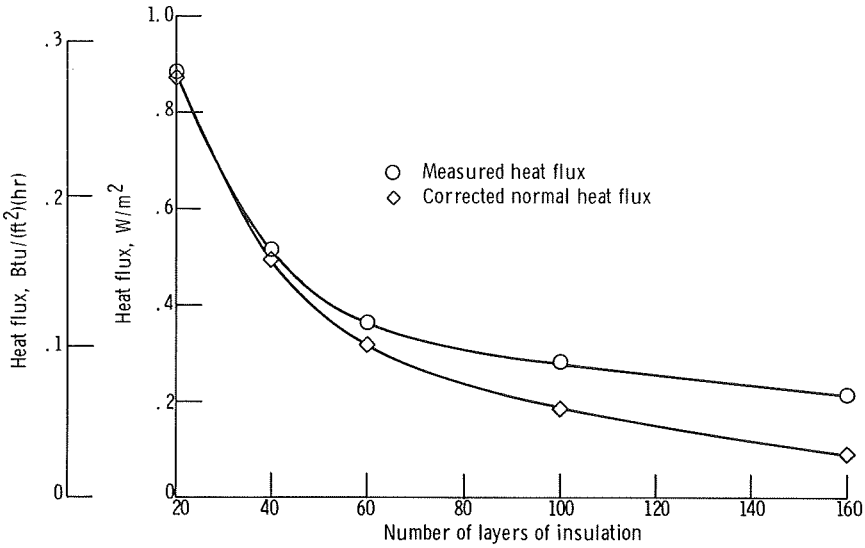

Figure 7. - Heat flux as function of number of layers of insulation.

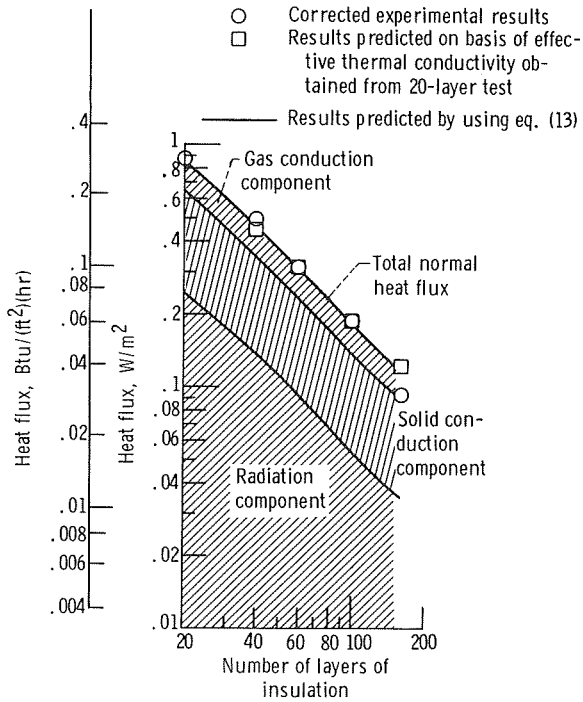

Figure 8. - Comparisons of experimental and predicted normal heat flux as function of number of layers of multilayer insulation.

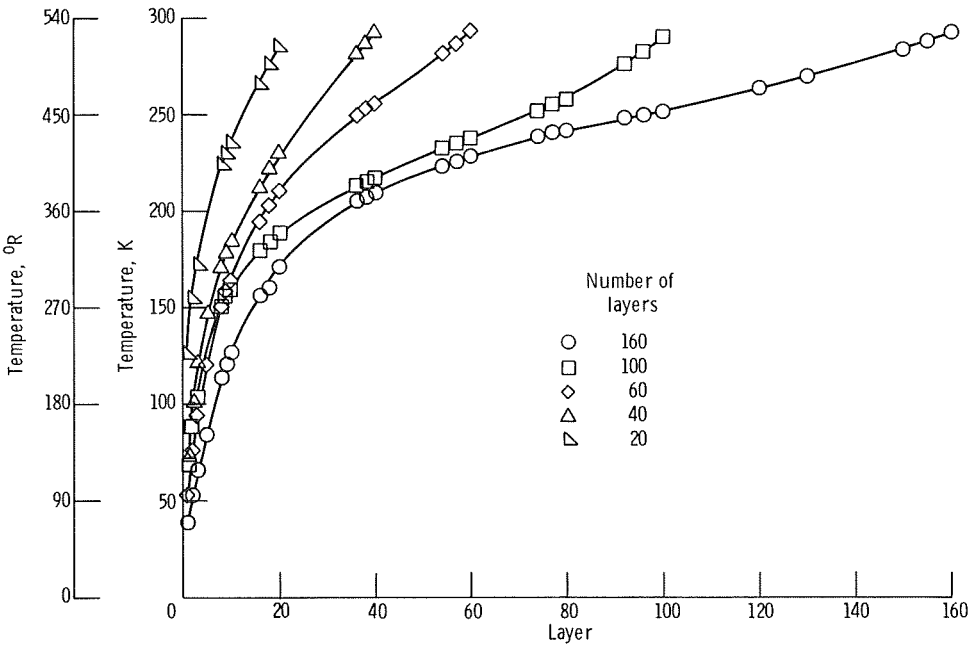

Figure 9. - Experimental temperature profiles through insulation for various numbers of layers.

NATIONAL AERONAUTICS AND SPACE ADMINISTRATION
WASHINGTON, D.C. 20546

OFFICIAL BUSINESS
PENALTY FOR PRIVATE USE $300

SPECIAL FOURTH-CLASS RATE
BOOK

POSTAGE AND FEES PAID
NATIONAL AERONAUTICS AND
SPACE ADMINISTRATION
451

U.S.MAIL

POSTMASTER : If Undeliverable (Section 158 Postal Manual) Do Not Return

"The aeronautical and space activities of the United States shall be conducted so as to contribute . . . to the expansion of human knowledge of phenomena in the atmosphere and space. The Administration shall provide for the widest practicable and appropriate dissemination of information concerning its activities and the results thereof."

—NATIONAL AERONAUTICS AND SPACE ACT OF 1958

NASA SCIENTIFIC AND TECHNICAL PUBLICATIONS

TECHNICAL REPORTS: Scientific and technical information considered important, complete, and a lasting contribution to existing knowledge.

TECHNICAL NOTES: Information less broad in scope but nevertheless of importance as a contribution to existing knowledge.

TECHNICAL MEMORANDUMS: Information receiving limited distribution because of preliminary data, security classification, or other reasons. Also includes conference proceedings with either limited or unlimited distribution.

CONTRACTOR REPORTS: Scientific and technical information generated under a NASA contract or grant and considered an important contribution to existing knowledge.

TECHNICAL TRANSLATIONS: Information published in a foreign language considered to merit NASA distribution in English.

SPECIAL PUBLICATIONS: Information derived from or of value to NASA activities. Publications include final reports of major projects, monographs, data compilations, handbooks, sourcebooks, and special bibliographies.

TECHNOLOGY UTILIZATION PUBLICATIONS: Information on technology used by NASA that may be of particular interest in commercial and other non-aerospace applications. Publications include Tech Briefs, Technology Utilization Reports and Technology Surveys.

Details on the availability of these publications may be obtained from:

SCIENTIFIC AND TECHNICAL INFORMATION OFFICE

NATIONAL AERONAUTICS AND SPACE ADMINISTRATION

Washington, D.C. 20546